

Thermodynamics of one and two-qubit quantum refrigerators interacting with squeezed baths: a comparative study

Ashutosh Kumar ^{*1} and Sourabh Lahiri ^{†1}

¹Birla Institute of Technology Mesra, Ranchi, Jharkhand 835215, India

Abstract

We investigate the nonequilibrium refrigeration of one and two-qubit systems in a squeezed thermal bath. We characterize the performance of one and two-qubit refrigerators in the presence of squeezed heat baths, in terms of their coefficients of performance, cooling rates, and figures of merit. Our results show that the performance of the refrigerators is strongly influenced by the squeezing parameter and the number of qubits. The performance of the two-qubit refrigerator is found to be better than that of the one-qubit refrigerator under the same operating conditions. Our findings suggest that a squeezed thermal bath can be a promising resource for the design of efficient quantum refrigerators in the non-equilibrium regime.

1 Introduction

Refrigerators are thermal devices that are useful for cooling a system. Over the last two decades, there has been a lot of study towards extending these macroscopic machines to microscopic scales [1–5]. They are likely to have a significant effect in energy harvesting at nanoscales and are predicted to have the potential of revolutionizing the pharmaceutical industry [6–8]. Tiny refrigerators have been shown to be useful in cooling AFM cantilevers [9] and in intramolecular cooling [10].

Typically, a Brownian particle trapped in a confining potential is used in classical stochastic thermal machines [1, 2, 11]. A lot of interest has been directed towards quantum heat engines, which have been shown to offer several advantages over their classical counterparts [12–15]. Pioneering work on quantum heat engine (QHE) was done in [16] that dealt with maser heat engines. In [17–20], the authors proposed models of a QHE within an open quantum system framework. Quantum thermodynamics [21] has become a standard framework for studying these machines.

A comparative study of the performance of one and two-qubit quantum engines in the presence of squeezed heat baths was done in [22], demonstrating that the two-qubit engines typically yield higher power. Additionally, by adjusting the squeezing parameters, the machine can be made to operate in either engine or in refrigerator mode.

*ashutoshkumarr06@gmail.com

†sourabhlahiri@gmail.com

The coefficient of performance (COP) is a measure of the quality of results delivered by a refrigerator or a heat pump. A higher COP indicates a more efficient system. An ideal candidate for optimizing the performance of a refrigerator is its figure of merit χ , which was first studied in [23]. It provides equal weightage to the COP of the refrigerator and its cooling rate (CR) and is an important parameter to determine how useful the device is. In [24], the authors study the optimization of χ and CR for a three-level atomic system.

Here, we study the one and two-qubit refrigerator in a nonequilibrium setup (finite cycle time) in the presence of squeezed thermal baths [25, 26]. This entails the use of the quantum master equation [27, 28]. The refrigerator protocol is obtained by time-reversing the Otto engine protocol of [22], so that the clear distinctions between the steps where work is done and those where heat is exchanged are retained. The functional dependences of the thermodynamic observables of the refrigerator on various parameters are studied, first for the one-qubit and then for the two-qubit system. We compare the qualitative and quantitative natures of the observables and study their similarities and differences. Generally, we find enhanced performances when two qubits constitute the working system - a result that was also observed when the engine protocol was applied to the system [22], even though a different set of thermodynamic observables were studied there.

The paper is organized as follows: In sec. 2, we discuss the model of one-qubit and two-qubit refrigerators. In Sec. 3, we define the thermodynamic observables. In sec. 4, we discuss the result of one-qubit refrigerators. Sec. 5 provides the corresponding study for two-qubit refrigerators. Finally, in Sec. 6, the key conclusions of this work are summarised and discussed.

2 Model

In this section, we describe the models used to study quantum refrigerators using a single qubit or two qubits as its working system. The refrigerator cycle considered is the reverse of the protocol used in [22] for a quantum heat engine, comprised of two thermodynamic processes - adiabatic and isochoric. Fig. 1 schematically shows such a cycle, given by the process $A \rightarrow B \rightarrow C \rightarrow D \rightarrow A$, labeled as strokes 1, 2, 3, and 4, respectively.

During the adiabatic compression step ($A \rightarrow B$), the energy gap between the two levels (for the two-qubit system, it is chosen as the mean energy gap of the two qubits) changes from ω_h to ω_c . The next step $B \rightarrow C$ is the isochoric one, where the system evolves in contact with the cold bath maintained at temperature T_c . The third step $C \rightarrow D$ consists of adiabatic expansion where ω_c is changed to ω_h , while the final step $D \rightarrow A$ is another isochoric one where the system evolves in contact with the hotter bath at temperature T_h . As is clear from the description, the evolution during the adiabatic steps are unitary, while those in the isochoric steps are non-unitary. In addition, the heat baths are subjected to squeezing, which is described by means of the squeezing parameters r and ϕ (to be elaborated below). We find the latter parameter to have no effects on the engine's output parameters. Further, the two heat baths are in general subject to different squeezing parameters: $r = r_h$ for the hotter bath, and $r = r_c$ for the colder bath. The effective temperature of the heat baths under the effect of squeezing can be shown to be given by $T_{h/c}^{\text{eff}} = T_{h/c} \cosh(2r_{h/c})$, as has been shown in [29] ($T_{h/c}$ is the actual thermal temperature of the hot/cold bath).

The evaluation of the mean energy of the one-qubit and two-qubit systems at the four corners of the cycle is necessary for the examination of the performance of the refrigerator. The average energy at any state α is $\langle E_\alpha \rangle \equiv \text{Tr}[\rho_\alpha H_\alpha]$, ρ_α being the reduced density matrix for the system and H_α being the Hamiltonian operator, with $\alpha = A, B, C$ or D . Further details are provided in Sec. 3.

2.1 Model for a one-qubit refrigerator (OQR)

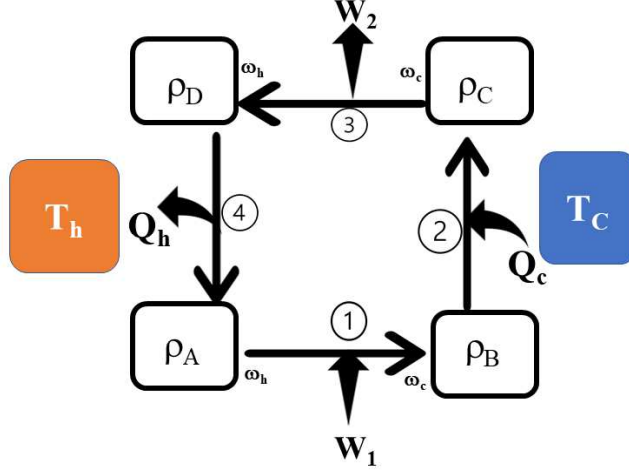


Fig. 1: An illustration of the one-qubit quantum Otto refrigerator cycle.

The Hamiltonian of the one-qubit system, in the z -basis, is given by

$$H(\omega(t)) = \frac{1}{2}\omega(t)\sigma_z. \quad (1)$$

Here, σ_z is the third Pauli matrix, and $\omega(t)$ is the time-dependent energy gap between the two energy levels. We now consider looking at the development of the density operator, which is represented by the von Neumann equations during the unitary steps $A \rightarrow B$ and $C \rightarrow D$, and by the Lindblad equations during the dissipative steps $B \rightarrow C$ and $D \rightarrow A$ (see Fig. 1). The density operator is a 2×2 matrix, which will be represented in the energy basis $\{|g\rangle, |e\rangle\}$ that correspond to the ground and the excited states, respectively.

Stroke 1, $A \rightarrow B$ (Adiabatic Compression): The frequency of the Hamiltonian is linearly modulated with time from ω_h to $\omega_c < \omega_h$ linearly in time:

$$\omega(t) = \omega_h(1 - t/\tau) + \omega_c t/\tau. \quad (2)$$

The von-Neumann equation is used to evolve the density matrix $\rho(t)$.

$$\frac{\partial \rho(t)}{\partial t} = -\frac{i}{\hbar}[H(\omega(t)), \rho(t)], \quad (3)$$

where

$$\sigma_z = \begin{pmatrix} 1 & 0 \\ 0 & -1 \end{pmatrix}. \quad (4)$$

(5)

The work done on the system in this process will be given by $W = \langle E_B \rangle - \langle E_A \rangle$. For convenience, in this article, we simplify the equations by setting Planck's constant and Boltzmann's constant to one (i.e., $\hbar = 1$, $k_B = 1$).

Stroke 2, B \rightarrow C (cold isochore): This is a non-unitary process (since the system is in contact with the cold thermal bath), and the final Hamiltonian at C is given by $H(\omega_c) = (\omega_c/2)\sigma_z$. Heat is absorbed from the cold bath by the system. The quantum master equation results in the evolution of the system's density matrix $\rho(t)$, which is shown below

$$\frac{\partial \rho(t)}{\partial t} = -\frac{i}{\hbar} [H(\omega_c), \rho(t)] + \sum_{j=1,2} \left[2R_j \rho(t) R_j^\dagger - \{R_j^\dagger R_j, \rho(t)\} \right], \quad (6)$$

where $R_1 = \left[\sqrt{\gamma_0(n_{th} + 1)/2} \right] R$, $R_2 = \left[\sqrt{\gamma_0 n_{th}/2} \right] R^\dagger$, and $R = \cosh(r)\sigma_- + \exp(i\phi)\sigma_+ \sinh(r)$, with r and ϕ being the squeezing parameters. The parameter γ_0 is the rate of spontaneous emission. $n_{th} = 1/(e^{\beta_c \omega_c} - 1)$ gives the average number of photons emitted with frequency ω_c and inverse temperature β_c . The curly brackets $\{A_1, A_2\}$ denote anti-commutation of operators A_1 and A_2 .

Stroke 3, C \rightarrow D (Adiabatic expansion): The system is now decoupled from the cold bath. The energy level spacing is changed linearly from ω_c to ω_h according to the protocol

$$\omega(t) = \omega_h(t/\tau - 2) + \omega_c(3 - t/\tau). \quad (7)$$

The density matrix $\rho(t)$ is again evolved using the von-Neumann equation (see Eq. (3)).

Stroke 4, D \rightarrow A (Hot isochore): The system is now coupled to the hot thermal bath. The Hamiltonian in this stroke is kept fixed at $H(\omega_h) = (\omega_h/2)\sigma_z$, with the energy gap held constant at ω_h . Again, the evolution of the state $\rho(t)$ is through the quantum master equation (see Eq. (6)). In this step, heat is released into the hot bath.

If the process is carried out quasistatically, the density operators at the states A, B, C, and D would correspond to the Boltzmann distribution, and the energy averages are easy to calculate in the absence of any squeezing:

$$\begin{aligned} \langle E_A \rangle &= \frac{-\omega_h}{2} \tanh\left(\frac{\beta_h \omega_h}{2}\right); \\ \langle E_B \rangle &= \frac{-\omega_c}{2} \tanh\left(\frac{\beta_h \omega_h}{2}\right); \\ \langle E_C \rangle &= \frac{-\omega_c}{2} \tanh\left(\frac{\beta_c \omega_c}{2}\right); \\ \langle E_D \rangle &= \frac{-\omega_h}{2} \tanh\left(\frac{\beta_h \omega_h}{2}\right). \end{aligned} \quad (8)$$

However, throughout this work, we will generally be dealing with a nonequilibrium engine, and the average energy at these states will be different from the equilibrium ones.

2.2 Model for a two-qubit refrigerator (TQR)

We now consider a refrigerator that uses a two-qubit system as the working medium that interacts with a squeezed thermal bath. An additional parameter emerges now, that would affect the performance of the refrigerator in this case. It is the distance r_{12} between qubit 1 and qubit 2. When the qubits are close enough (see below), they interact collectively with the bath and are thus said to be in the collective regime. For much larger distances between them, they are said to be in an independent regime.

Let the energy level spacings of qubits 1 and 2 be given by $\omega_1(t)$ and $\omega_2(t)$, respectively. The evolution of the density matrix of the two-qubit system is given by [22, 25, 27]

$$\frac{\partial \rho(t)}{\partial t} = -\frac{i}{\hbar}[\tilde{H}, \rho(t)] - L_1(\rho) - L_2(\rho) + L_3(\rho) + L_4(\rho), \quad (9)$$

where the operator \tilde{H} is as defined in Eq. (14), and

$$\begin{aligned} L_1(\rho) &= \frac{1}{2}\Gamma_{12} \sum_{i,j=1}^2 (1 + N_{th}[\cosh^2(r) + \sinh^2(r)] + \sinh^2(r))(\rho S_i^+ S_j^- + S_i^+ S_j^- \rho - 2S_j^- \rho S_i^+); \\ L_2(\rho) &= \frac{1}{2}\Gamma_{12} \sum_{i,j=1}^2 (N_{th}[\cosh^2(r) + \sinh^2(r)] + \sinh^2(r))(\rho S_i^- S_j^+ + S_i^- S_j^+ \rho - 2S_j^+ \rho S_i^-); \\ L_3(\rho) &= \frac{1}{2}\Gamma_{12} \sum_{i,j=1}^2 \left(-\frac{1}{2} \sinh(2r) \exp(i\phi)\right)(2N_{th} + 1)(\rho S_i^+ S_j^+ + S_i^+ S_j^+ \rho - 2S_j^+ \rho S_i^+); \\ L_4(\rho) &= \frac{1}{2}\Gamma_{12} \sum_{i,j=1}^2 \left(-\frac{1}{2} \sinh(2r) \exp(-i\phi)\right)(2N_{th} + 1)(\rho S_i^- S_j^- + S_i^- S_j^- \rho - 2S_j^- \rho S_i^-), \end{aligned}$$

$$\begin{aligned} N_{th} &= \frac{1}{\exp(\hbar\omega_0/k_B T) - 1}; \\ \omega_0 &= \frac{\omega_1 + \omega_2}{2}. \end{aligned} \quad (10)$$

Here, ω_{1h} , ω_{2h} , ω_{1c} , and ω_{2c} correspond to the different level spacings of the independent one-qubit systems (just as in the case of the OQR), except that an extra index (1 and 2) indicate whether the state is of qubit 1 or qubit 2. We further define: $\omega_{0h} = (\omega_{1h} + \omega_{2h})/2$ and $\omega_{0c} = (\omega_{1c} + \omega_{2c})/2$. The time-dependence of the Hamiltonian comes through the parameter $\omega_0(t)$ that replaces $\omega(t)$ in Eq. (7), where ω_{0h} and ω_{0c} are substituted for ω_h and ω_c , respectively. r and ϕ are the squeezing parameters and Γ_{12} is the collective spontaneous emission rate given in terms of individual spontaneous emission rates Γ_1 and Γ_2 :

$$\Gamma_{12} = \Gamma_{21} = \sqrt{\Gamma_1 \Gamma_2} F(k_0 r_{12}), \quad (11)$$

where

$$\Gamma_i = \frac{\omega_i^3 \mu_i^2}{3\pi\epsilon\hbar c^3}, \quad (i = 1, 2), \quad r_{12} = |\mathbf{r}_{12}| = r_{21}, \quad k_0 = \omega_0/c, \quad (12)$$

$$F(k_0 r_{12}) = \frac{3}{2} \left[\{1 - (\hat{\boldsymbol{\mu}} \cdot \hat{\mathbf{r}}_{12})^2\} \frac{\sin(k_0 r_{12})}{(k_0 r_{12})} + \{1 - 3(\hat{\boldsymbol{\mu}} \cdot \hat{\mathbf{r}}_{12})^2\} \times \left\{ \frac{\cos(k_0 r_{12})^2}{(k_0 r_{12})} - \frac{\sin(k_0 r_{12})}{(k_0 r_{12})^3} \right\} \right]. \quad (13)$$

Here, $\mathbf{r}_{12} \equiv (\mathbf{r}_2 - \mathbf{r}_1)\omega_0/c$ is the normalized displacement vector of the second spin with respect to the first. The dipole moments of atomic transition are given by $\boldsymbol{\mu}_1$ and $\boldsymbol{\mu}_2$. The hats represent unit vectors. For identical qubits that are considered in our case, $\Gamma_1 = \Gamma_2 = \Gamma$ and $\mu_1 = \mu_2 = \mu$. The dynamics of the system in contact with the cold bath follow similar equations. The Hamiltonian \tilde{H} appearing in the Eq. (9) is given by

$$\tilde{H} = \hbar(\omega_1 S_1^z + \omega_2 S_2^z) + \hbar\Omega_{12}(S_1^+ S_2^- + S_2^+ S_1^-), \quad (14)$$

where

$$\begin{aligned} S_1^z &= \frac{1}{2}(|e_1\rangle\langle e_1| - |g_1\rangle\langle g_1|); & S_2^z &= \frac{1}{2}(|e_2\rangle\langle e_2| - |g_2\rangle\langle g_2|) \\ S_1^+ &= |e_1\rangle\langle g_1|, & S_2^+ &= |e_2\rangle\langle g_2|; & S_1^- &= |g_1\rangle\langle e_1|, & S_2^- &= |g_2\rangle\langle e_2|. \\ \Omega_{12} = \Omega_{21} &= \frac{3}{4}\Gamma \left[-\{1 - (\hat{\boldsymbol{\mu}} \cdot \hat{\mathbf{r}}_{12})^2\} \frac{\cos(k_0 r_{12})}{(k_0 r_{12})} + \{1 - 3(\hat{\boldsymbol{\mu}} \cdot \hat{\mathbf{r}}_{12})^2\} \times \left\{ \frac{\sin(k_0 r_{12})^2}{(k_0 r_{12})} + \frac{\cos(k_0 r_{12})}{(k_0 r_{12})^3} \right\} \right]. \end{aligned} \quad (15)$$

The convenient basis that diagonalizes the \tilde{H} , also called the dressed state basis, is given by:

$$\begin{aligned} |g\rangle &= |g_1\rangle|g_2\rangle, \\ |s\rangle &= \frac{1}{\sqrt{2}}(|e_1\rangle|g_2\rangle + |g_1\rangle|e_2\rangle), \\ |a\rangle &= \frac{1}{\sqrt{2}}(|e_1\rangle|g_2\rangle - |g_1\rangle|e_2\rangle), \\ |e\rangle &= |e_1\rangle|e_2\rangle. \end{aligned} \quad (16)$$

The eigenvalues are respectively given by $E_g = -\hbar\omega_0$, $E_s = \hbar\Omega_{12}$, $E_a = -\hbar\Omega_{12}$ and $E_e = \hbar\omega_0$. The differential equations followed by each element of the density matrix are provided in [22,26]. We simulate these equations to obtain the evolution of the density matrix.

3 Important thermodynamic quantities

1. **Work:** In the analysis of any heat engine/refrigerator, the output work is of fundamental importance. The unitary processes ($A \rightarrow B$ and $C \rightarrow D$) constitute the steps where work is done on/by the system. The works retrieved from the system in these two processes are given by

$$\langle W_{AB} \rangle = \langle E_B \rangle - \langle E_A \rangle; \quad \langle W_{CD} \rangle = \langle E_D \rangle - \langle E_C \rangle. \quad (17)$$

2. **Heat:** The heat absorbed by the system in the non-unitary steps is defined as (a negative value would indicated heat dissipated):

$$\langle Q_{BC} \rangle = \langle E_C \rangle - \langle E_B \rangle; \quad \langle Q_{DA} \rangle = \langle E_A \rangle - \langle E_D \rangle. \quad (18)$$

3. **Coefficient of Performance:** A refrigerator's *coefficient of performance* (ζ) is obtained by dividing the heat extracted from the cold reservoir by the total work:

$$\zeta = \frac{\langle Q_c \rangle}{\langle W \rangle} = \frac{\omega_c}{\omega_h - \omega_c}, \quad (19)$$

whose derivation has been derived in appendix A.

4. **Cooling rate:** It is defined as the heat absorbed from the cold bath divided by the cycle time:

$$CR = \frac{\langle Q_c \rangle}{\tau_{\text{cycle}}} \quad (20)$$

We define the maximum value of CR with respect to ω_c as the maximum cooling rate, CR_{max} [24].

5. **Figure of merit (χ):** The figure of merit χ is defined as the product of heat absorbed from the cold reservoir $\langle Q_c \rangle$ and the coefficient of performance (ζ) divided by the cycle time [23] :

$$\begin{aligned} \chi &= \frac{\langle Q_c \rangle \zeta}{\tau_{\text{cycle}}} \\ &= CR \times \zeta. \end{aligned} \quad (21)$$

3.1 Quasistatically driven one-qubit refrigerator in absence of squeezing

We now derive a few analytical expressions in the absence of squeezing of either the hot or the cold baths ($r_h = r_c = 0$), which we use as benchmarks for our simulations. If we use the expressions for equilibrium steady state in the absence of squeezing, namely Eq. (8), then the CR is given by

$$CR = \frac{-\frac{1}{2}\omega_c \tanh\left(\frac{\beta_c \omega_c}{2}\right) + \frac{1}{2}\omega_c \tanh\left(\frac{\beta_h \omega_h}{2}\right)}{\tau_{\text{cycle}}}, \quad (22)$$

which leads to the maximum cooling rate CR_{max} by equating $\frac{d(CR)}{d\omega_c}$ to 0:

$$CR_{\text{max}} = \frac{\frac{1}{4}\beta_c \omega_c^2 \operatorname{sech}\left(\frac{\beta_c \omega_c}{2}\right)^2}{\tau_{\text{cycle}}}. \quad (23)$$

The expression for the figure of merit is given by

$$\chi = \frac{\omega_c \left[-\frac{1}{2} \left(\omega_c \tanh\left(\frac{\beta_c \omega_c}{2}\right) + \omega_c \tanh\left(\frac{\beta_h \omega_h}{2}\right) \right) \right]}{(\omega_h - \omega_c) \tau_{\text{cycle}}}. \quad (24)$$

χ at the maximum cooling rate (MCR) can be readily computed. The following expression is obtained:

$$\chi_{\text{MCR}} = \frac{\omega_c \left[\frac{1}{4} \beta_c \omega_c^2 \operatorname{sech}\left(\frac{\beta_c \omega_c}{2}\right)^2 \right]}{(\omega_h - \omega_c) \tau_{\text{cycle}}}. \quad (25)$$

4 Results and Discussions for one-qubit refrigerator

We now study the thermodynamics of the OQR and later use the results for comparison when we study the TQR in the next section. The squeezing parameter ϕ has no effect on the output, so we set them to zero throughout our analysis. Therefore, a reference to the squeezing parameter would solely refer to the parameter r (with subscripts h and c , in order to indicate the bath in whose contact the system is evolving) in Eq. (6).

Comparison with analytics: In order to benchmark our codes, we compare the analytical expressions obtained from Eqs. (19) and (22) with the results obtained from our simulations in Figs. 2(a) and (b), respectively. The symbols indicate results obtained from our simulations, while the solid line is the result obtained from analytics. Fig. 2(a) shows an excellent agreement between the analytical (see Eq. (19)) and simulated values of the coefficient of performance ζ . Similar degree of agreement is observed between the analytical (see Eq. (22)) and simulated values of CR in Fig. 2(b), in absence of squeezing ($r_h = 0, r_c = 0$) and in the limit of quasistatic driving. This establishes the accuracy of our simulations, thereby benchmarking our code.

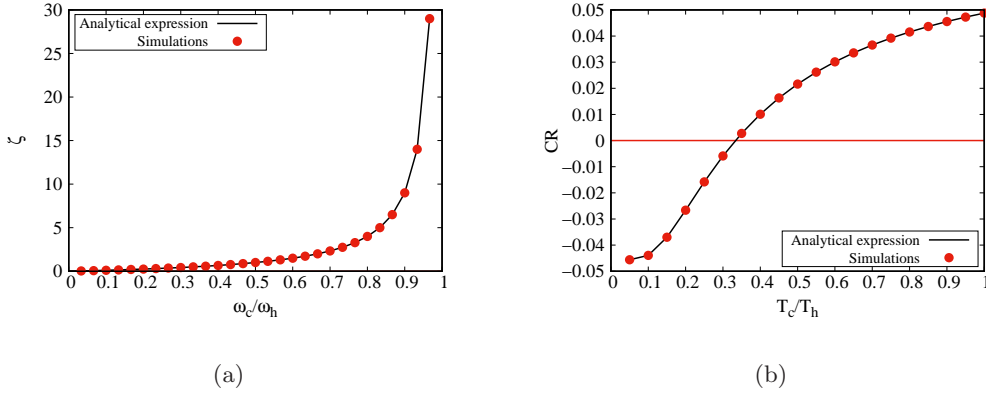


Fig. 2: (a) The behavior of ζ as a function of ω_c/ω_h , obtained from simulations (denoted by symbols) as well as analytics (solid line) in the absence of squeezing. (b) Comparison between analytical expression and simulations of CR as a function of T_c/T_h in the quasistatic limit at $r_h = r_c = 0$. Other parameters are : $\omega_h = 30, \omega_c = 10, \gamma_0 = 1, \tau = 10$.

Cooling rate of Refrigerator:- Fig. 3 (a) shows the dependence of CR on the temperature ratio T_c/T_h , for different values of the squeezing parameters r_c and r_h . When the temperature ratio increases, i.e., the temperature difference reduces, the CR is observed to increase. This is in accordance with our expectations: a decrease in thermal gradient helps the refrigerator to pump heat against it. The curves shown in the figure are for different values of the squeezing parameters r_h and r_c , as mentioned in the legends. The device no longer functions as a refrigerator below the line $CR = 0$ (horizontal red line). The third curve from the top (black line with solid squares) is that of a thermal quantum refrigerator in the absence of squeezing, which serves as a reference. As long as $r_h < r_c$, the refrigerator performs better than the thermal refrigerator, implying that the effective temperature of the cold bath has increased with respect to the increase in the temperature of the hot bath. In the opposite regime, $r_h > r_c$ (cyan curve with pentagons), the refrigerator becomes more inefficient than the normal refrigerator. Fig. 3 (b) shows the variation

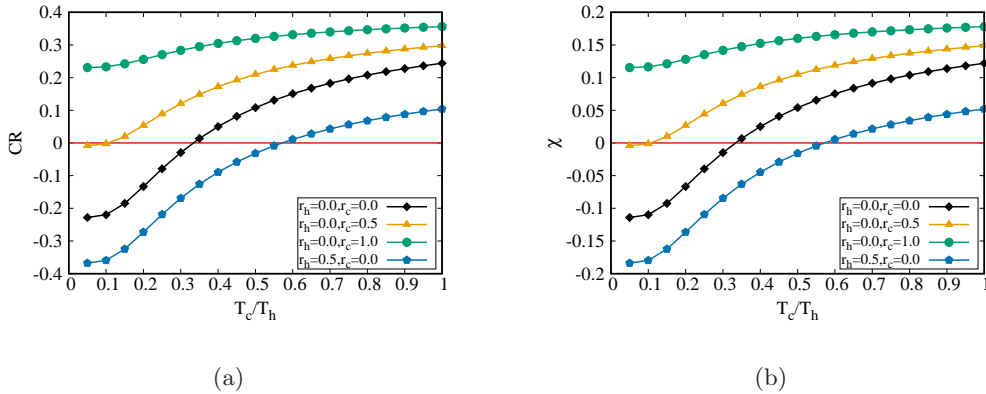


Fig. 3: Variation of (a) CR and (b) χ of an OQR as a function of the temperature ratio T_c/T_h for different sets of r_h and r_c . Other parameters are : $\omega_h = 30$, $\omega_c = 10$, $\gamma_0 = 1$.

of the figure of merit χ with T_c/T_h for the same set of parameters. Note that with ω_c/ω_h fixed, the coefficient of performance ζ becomes a constant. Thus, from Eq. (22) and (24), it is easy to see that ζ will be proportional to χ , thereby exhibiting exactly the same qualitative trends.

In figure 4(a), variation of CR as a function of the ratio of energy gaps ω_c/ω_h has been shown for different sets of the squeezing parameter r_c and r_h . The other parameters are as mentioned in the figure caption. It can be clearly seen that whether the curve shows non-monotonicity or acts as a refrigerator at all, strongly depends on the ratio of energy gaps. As r_c increases compared to r_h , the range of values of ω_c/ω_h in which the system is in the refrigerator mode (i.e., the curves remain above the $CR = 0$ line) increases. For high enough values of r_c , the non-monotonicity vanishes completely. The black curve, as before, is the reference line in the absence of squeezing: $r_h = r_c = 0$. As expected, it is observed that the case in which r_h exceeds r_c under-performs with respect to this normal refrigerator, due to the increased thermal drive acting on the system in the opposite direction. Fig. 4(b) shows the functional dependence of CR again on the ratio ω_c/ω_h , but this time the squeezing parameters are kept constant and the temperature ratio T_c/T_h is varied to obtain the different curves. The non-monotonicity in all the curves is apparent. These plots can be used to obtain the figure of merit at the maximum cooling rate, χ_{MCR} , as well as the coefficient of performance at the maximum cooling rate, ζ_{MCR} . These are useful parameters that quantify the performance of a refrigerator [23, 30–32], similar to the efficiency at maximum power for an engine. These parameters have been explored next.

χ and ζ at the maximum cooling rate: Figs. 5(a) and (b) show the variations in χ_{MCR} and ζ_{MCR} respectively with the ratio of bath temperatures. Both the quantities increase with the increase in T_c/T_h , and the increase is higher when the squeezing of the cold bath is more (i.e., the value of r_c is higher). This is because, as can be observed from the plots of Fig. 4(b), the maximum CR occurs at values of ω_c/ω_h that increase with the increase in T_c/T_h . Since ζ monotonically increases with ω_c/ω_h (see Fig. 2(a)), it can be readily inferred that the values of ζ at these maxima must increase as well with T_c/T_h .

Phase plots: The phase plot of OQR, showing the variation of CR with the values of ω_c/ω_h (vertical axis) and T_c/T_h (horizontal axis), has been provided in Fig. 6(a). The non-monotonic behavior with respect to ω_c/ω_h for fixed values of T_c/T_h is apparent, which is consistent with

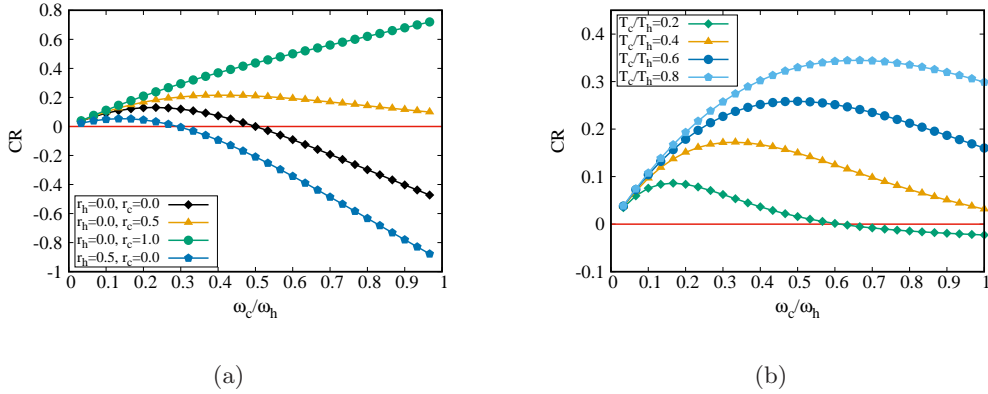


Fig. 4: (a) Variation of CR of an OQR as a function of the ω_c/ω_h for different r_c and r_h . Other parameters are $T_h = 20$, $T_c = 10$, $\gamma_0 = 1$. (b) Variation of the CR as the function of ω_c/ω_h for different T_c/T_h at $r_c = 0.5$ and $r_h = 0$.

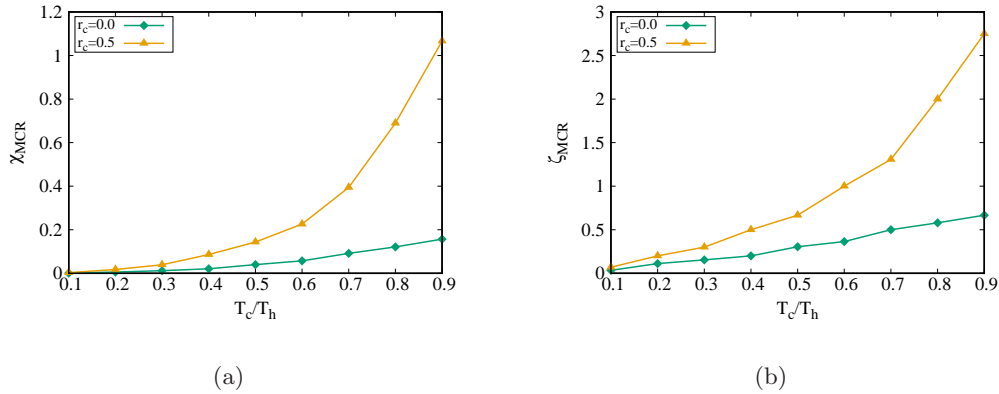


Fig. 5: (a) Variation of χ_{MCR} with T_c/T_h , and (b) Variation of ζ_{MCR} with T_c/T_h , for $r_c = 0$ and 0.5 . Other parameters are $r_h = 0$, $\gamma_0 = 1$, $\omega_c = 10$, $\omega_h = 30$.

the results shown in Fig. 4(b). Fig. 6(b) gives the phase plot of the variations in CR with the squeezing parameters r_h and r_c . Agreement with Fig. 4(a) is observed in this case, showing that the effective temperature of a bath rises with the increase in squeezing, and vice versa.

5 Results and Discussions on TQR

We now examine the two-qubit refrigerator, whose dynamics were explained in Sec. 2.2, and compare the thermodynamic observables with those of OQR. We demonstrate that the TQR turns out to be a better choice in terms of the usefulness of the refrigerator. The parameter ϕ is found to have no effects on the refrigerator outputs, just as in the case of the OQR. Consequently, we again deal only with the parameter r , with subscripts h and c indicating the concerned bath. The other parameters that we keep fixed are the time duration of each stroke of the refrigerator cycle, $\tau = 2$, and the spontaneous emission rates $\Gamma_1 = \Gamma_2 = \Gamma$, which we set to unity (refer to

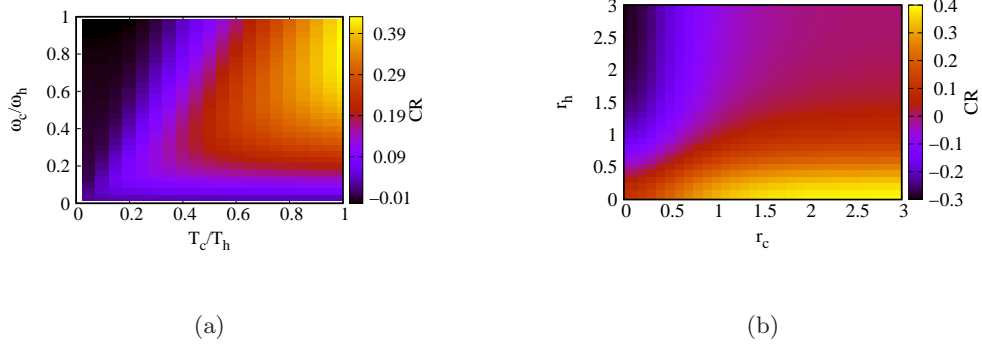


Fig. 6: (a) Phase plot of CR of an OQR as a function of T_c/T_h and ω_c/ω_h . The parameters used are $r_c = 0.5$, and $r_h = 0$. (b) Phase plot showing the CR varies depending on the r_c and r_h . Other parameter are $\gamma_0 = 1$, $\omega_c = 10$, $\omega_h = 30$, $T_h = 20$, $T_c = 10$.

Eq. (11)). The working of a TQR can be divided into two regimes. If the normalized distance r_{12} (given by the ratio of the actual distance to $2\pi/k_0$) between the qubits is large, $r_{12} > 1$, the regime is called *independent* decoherence regime, while if $r_{12} \ll 1$, the regime is called *collective* decoherence regime.

Cooling rate :- Fig. 7 shows the variation of CR with the ratio of bath temperatures T_c/T_h in the decoherence regime. We find the trend to be very similar to that of Fig. 4. However, there are substantial quantitative differences in favor of the TQR, as can be observed from the high values of CR reached for similar values of the other parameters (see caption for the values of the set of parameters used). The effect of different combinations of r_h and r_c once again underscores the role played by these parameters in deciding the effective temperatures of the heat baths.

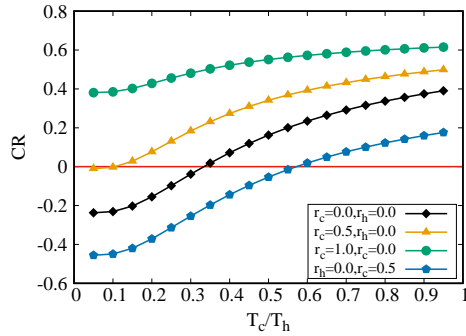


Fig. 7: Variation of CR of a TQR as a function of the temperature ratio T_c/T_h for different squeezed parameters r_h and r_c . Other parameters are : $\omega_{0h} = 30$, $\omega_{0c} = 10$, $\Gamma = 1$, $r_{12} = 0.5$.

Figs. 8(a) and (b) show the variations in CR with the ratios ω_{0c}/ω_{0h} and T_c/T_h respectively,

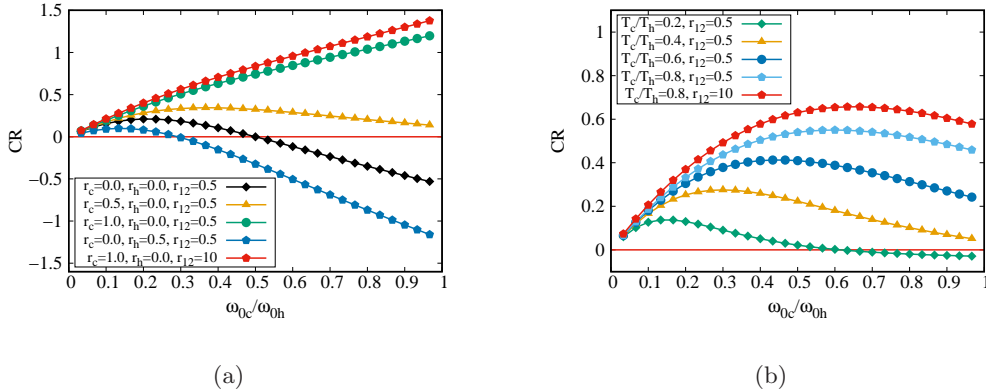


Fig. 8: (a) Variation of CR of a TQR as a function of ω_c/ω_h for different values of r_c and r_h . (b) CR as the function of ω_c/ω_h for different values of T_c/T_h with $r_c = 0.5$ and $r_h = 0$. Other parameters are $T_h = 20$, $T_c = 10$, $\Gamma = 1$, $r_{12} = 0.5$ for four curves from bottom and $r_{12} = 10$ for first curve from top.

for the same parameters used for OQR. In both the subfigures, the first four curves from below are for the qubit being in the collective decoherence regime ($r_{12} \ll 1$, whose value we have chosen to be 0.5) for fixed values of squeezing parameters, while the upper plot (red solid line with solid pentagons) shows this functional dependence in the independent decoherence regime ($r_{12} > 1$, whose value we have chosen to be 10). In the independent decoherence regime, the TQR is found to yield higher values of CR . This effect can be explained as follows. As shown in [25], the number of decay channels for the system is higher in the independent decoherence regime. This in turn implies that both the absorption and dissipation of heat take place at a higher rate in this regime as compared to the collective decoherence regime, thereby leading to enhanced values of CR . Comparing with Figs. 4(a) and (b) respectively, similar qualitative trends but with higher values of CR are observed.

The higher values of CR for a TQR can be heuristically argued as follows. Since out of the total number of particles in the ensemble distributed in all four levels, the lower two levels contain a bigger fraction as compared to the fraction of particles present in the ground state of a two-level system [22, 29]. Since the levels are closer when in contact with the cold reservoir, the above fact leads to a higher probability of particles getting excited by absorbing heat from the colder reservoir, thereby leading to higher values of $\langle Q_c \rangle$ for the TQR.

ζ and χ at maximum cooling rate: The procedure used to determine ζ_{MCR} and χ_{MCR} at the maximum cooling rate is the same as that used for the OQR. Fig. 9(a) shows χ_{MCR} as a function of T_c/T_h for unsqueezed baths in the independent (upper curve) and collective (lower curve) decoherence regimes. Fig. 9(b) provides similar curves when the cold bath is squeezed ($r_c = 0.5$), showing substantial improvement over Fig. 9(a). Fig. 9(c) shows the variation of ζ_{MCR} with the temperature ratio. In all the sub-figures, the independent decoherence regime is more conducive to the refrigerator's performance. Noting that since the maximum of CR occurs at a higher value of ω_c/ω_h in the independent decoherence regime (see Fig. 8(b)), we expect (one may refer to Eq. (25) for the quasistatically driven OQR as an approximate indicator of this qualitative nature) higher values of χ_{MCR} and ζ_{MCR} in the independent decoherence regime. The simulations are observed to conform to our expectations.

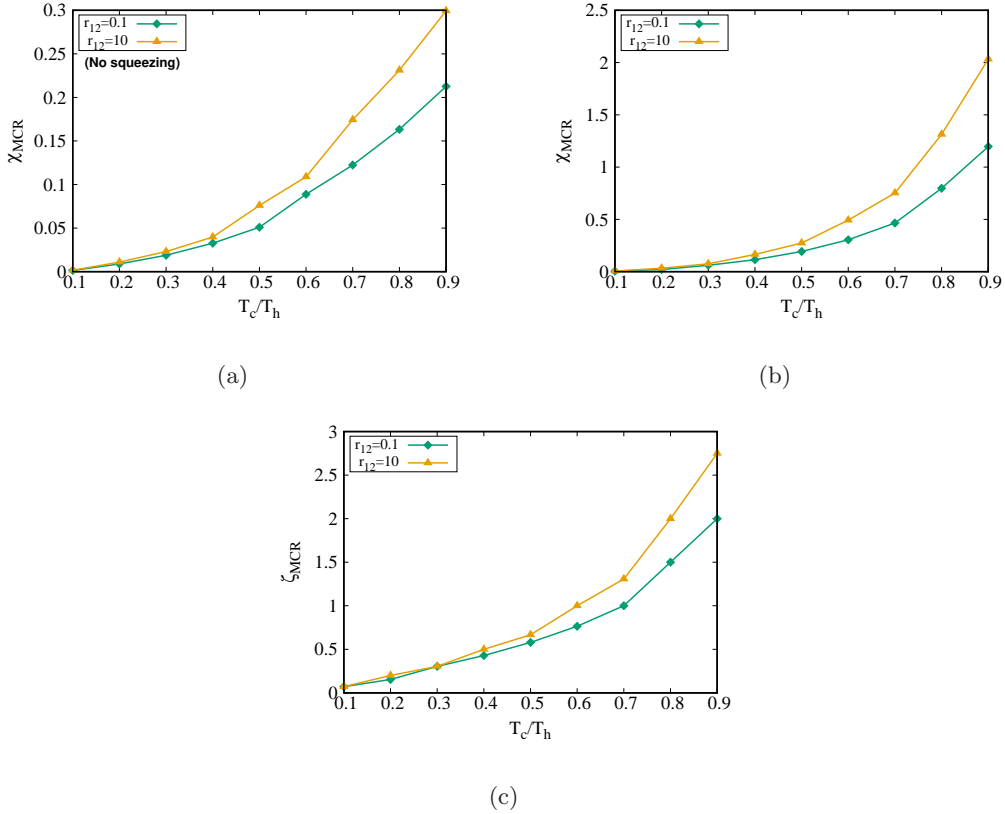


Fig. 9: (a) Show the figure of merit χ_{MCR} as function of T_c/T_h in the collective regime ($r_{12} = 0.1$) and independent decoherence regime ($r_{12} = 10$) for $r_h = 0$ and $r_c = 0$. (b) Same plot as in 9(a) for $r_h = 0$ and $r_c = 0.5$ (c) Show the ζ_{MCR} as function of T_c/T_h in the collective decoherence regime ($r_{12} = 0.1$) and independent decoherence regime ($r_{12} = 10$) for $r_h = 0$ and $r_c = 0.5$. Other parameter are $\Gamma = 1$, $\omega_{0c} = 10$, $\omega_{0h} = 30$.

In Fig. 10(a), the CR as functions of ω_c/ω_h and T_c/T_h have been depicted by means of a phase plot. We observe that the non-monotonicity that was obtained in Fig. 6(a) for the OQR is also present in the case of the TQR. Fig. 10(b) provides the functional dependence of CR on r_c and r_h in the decoherence regime, which again shows similar qualitative trends as OQR. In both figures (a) and (b), the TQR quantitatively yields higher values of CR .

6 Conclusions

In this work, we have investigated one and two-qubit refrigerators in the presence of squeezed thermal reservoirs, and have made a comparative study of these systems. We have first described the model and theory of OQR and TQR. We have also derived the analytical expressions for the thermodynamics observables in the limit of quasistatic driving when squeezing is absent. Our simulations have been shown to agree with these results to very good accuracy. We have shown that the cooling rate CR as well as the figure of merit χ increase monotonically with the temperature ratio T_c/T_h , for both OQR and TQR. The coefficient of performance ζ is found

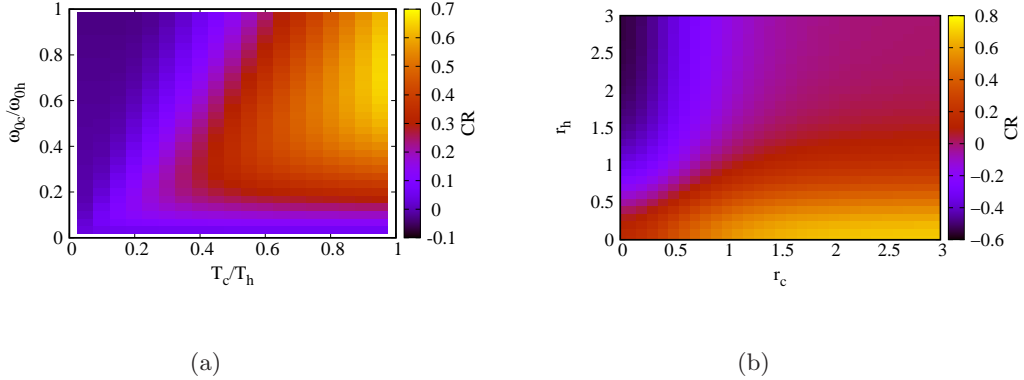


Fig. 10: (a) Phase plot of CR of a TQR as a function of T_c/T_h and ω_{0c}/ω_{0h} for $r_c = 0.5$, $r_h = 0$. (b) Phase plot showing the CR varies depending on the r_c and r_h . Other parameter are $\Gamma = 1$, $\omega_{0c} = 10$, $\omega_{0h} = 30$, $T_h = 20$, $T_c = 10$.

to be dependent on the ratio of energy level spacings ω_c/ω_h of the system, but independent of the squeezing parameters. However, the squeezing parameters affect both CR and χ , the latter being proportional to the former, where the constant of proportionality is ζ . As a function of the ratio of energy level spacings, the cooling rate shows a non-monotonic variation, with the general observation that it reaches higher values in the case of the TQR. These curves have been studied for different values of squeezing parameters as well as of T_c/T_h . From these plots, the values of χ_{MCR} and ζ_{MCR} have been extracted and plotted as a function of the temperature ratio. In accordance with our expectations, the curve for $r_c > 0$ shows higher values of these parameters, for both OQR and TQR. Phase plots have been plotted, showing the dependence of CR on T_c/T_h and ω_c/ω_h , as well as on r_c and r_h . Once again, the TQR outperforms the OQR. An additional parameter in the case of TQR is the normalized distance r_{12} between the two qubits. The values of χ_{MCR} and ζ_{MCR} are shown to be greater in the independent decoherence regime ($r_{12} > 1$), as compared to the collective decoherence regime ($r_{12} \ll 1$), owing to the increased number of decay channels in the former case. It would be interesting to check whether increasing the number of spins of the working system induces its thermodynamic behavior to converge towards that of a multi-state system like the quantum harmonic oscillator [19, 20].

7 Acknowledgement

One of us (AK) thanks A. Kumari for providing valuable insights through stimulating discussions.

A Derivation of coefficient of performance

We carry out the derivation for the OQR in details, and then state the result for the TQR. The average heat $\langle Q_{BC} \rangle$ absorbed from the cold bath in the system from B to C is given by

$$\langle Q_{BC} \rangle = \text{Tr}[(\rho_1 - \rho_0)H(\omega_c)]; \quad (26)$$

where $\rho_0 = \rho_A = \rho_B$ and $\rho_1 = \rho_C = \rho_D$ represent the density operators at A, B, C, and D.

Total work done is given by:

$$\begin{aligned}\langle W \rangle &= \langle W_{AB} \rangle + \langle W_{CD} \rangle \\ &= \text{Tr}[(\rho_1 - \rho_0)\{H(\omega_h) - H(\omega_c)\}]\end{aligned}\quad (27)$$

using the equation (26) and (27), coefficient of performance (ζ)

$$\begin{aligned}\zeta &= \frac{\langle Q_c \rangle}{\langle W \rangle} \\ &= \frac{\text{Tr}[(\rho_1 - \rho_0)H(\omega_c)]}{\text{Tr}[(\rho_1 - \rho_0)\{H(\omega_h) - H(\omega_c)\}]} \\ &= \frac{\text{Tr}[(\Delta\rho)H(\omega_c)]}{\text{Tr}[(\Delta\rho)\{H(\omega_h) - H(\omega_c)\}]}\end{aligned}\quad (28)$$

where, $(\rho_1 - \rho_0) \equiv \Delta\rho$
Now let

$$\Delta\rho = \begin{pmatrix} a & 0 \\ 0 & b \end{pmatrix}.$$

We also know,

$$\begin{aligned}H(\omega_c) &= \begin{pmatrix} \omega_c/2 & 0 \\ 0 & -\omega_c/2 \end{pmatrix}, \\ H(\omega_h) &= \begin{pmatrix} \omega_h/2 & 0 \\ 0 & -\omega_h/2 \end{pmatrix}.\end{aligned}$$

Then,

$$\begin{aligned}\text{Tr}[(\Delta\rho)H(\omega_c)] &= \omega_c \left(\frac{a-b}{2} \right) \\ \text{Similarly, } \text{Tr}[(\Delta\rho)H(\omega_h)] &= \omega_h \left(\frac{a-b}{2} \right)\end{aligned}\quad (29)$$

putting these relations into Eq. (28), we get the coefficient of performance(ζ)

$$\zeta = \frac{\omega_c}{\omega_h - \omega_c}.\quad (30)$$

For the TQR, we have verified separately that ζ exhibits a similar functional dependence on ω_{0c} and ω_{0h} :

$$\zeta \equiv \frac{\omega_{0c}}{\omega_{0h} - \omega_{0c}}.\quad (31)$$

References

- [1] Valentin Blickle and Clemens Bechinger. Realization of a micrometer-sized stochastic heat engine. *Nat. Phys.*, 8(2):143–146, 2012.
- [2] Tim Schmiedl and Udo Seifert. Efficiency at maximum power: An analytically solvable model for stochastic heat engines. *EPL*, 81(2):20003, 2007.

- [3] Aradhana Kumari, PS Pal, Arnab Saha, and Sourabh Lahiri. Stochastic heat engine using an active particle. *Phys. Rev. E*, 101(3):032109, 2020.
- [4] Aradhana Kumari and Sourabh Lahiri. Microscopic thermal machines using run-and-tumble particles. *Pramana*, 95:1–12, 2021.
- [5] Rui Long and Wei Liu. Performance of quantum otto refrigerators with squeezing. *Phys. Rev. E*, 91(6):062137, 2015.
- [6] AS Bhat. Nanobots: the future of medicine. *Int. J. Manag. Sci. Eng. Manag.*, 5(1):44–49, 2014.
- [7] Apoorva Manjunath and Vijay Kishore. The promising future in medicine: nanorobots. *j. biomed. sci. eng.*, 2(2):42–47, 2014.
- [8] Robert A Freitas. Pharmacytes: An ideal vehicle for targeted drug delivery. *J. Nanosci. Nanotechnol.*, 6(9-10):2769–2775, 2006.
- [9] Shoudan Liang, David Medich, Daniel M Czajkowsky, Sitong Sheng, Jian-Yang Yuan, and Zhifeng Shao. Thermal noise reduction of mechanical oscillators by actively controlled external dissipative forces. *Ultramicroscopy*, 84(1-2):119–125, 2000.
- [10] Hans J Briegel and Sandu Popescu. Entanglement and intra-molecular cooling in biological systems? A quantum thermodynamic perspective. *arXiv:0806.4552*, 2008.
- [11] Shubhashis Rana, PS Pal, Arnab Saha, and AM Jayannavar. Single-particle stochastic heat engine. *Phys. Rev. E*, 90(4):042146, 2014.
- [12] Noah Linden, Sandu Popescu, and Paul Skrzypczyk. How small can thermal machines be? The smallest possible refrigerator. *Phys. Rev. Lett.*, 105(13):130401, 2010.
- [13] Nicolas Brunner, Marcus Huber, Noah Linden, Sandu Popescu, Ralph Silva, and Paul Skrzypczyk. Entanglement enhances cooling in microscopic quantum refrigerators. *Phys. Rev. E*, 89(3):032115, 2014.
- [14] Johannes Roßnagel, Obinna Abah, Ferdinand Schmidt-Kaler, Kilian Singer, and Eric Lutz. Nanoscale heat engine beyond the carnot limit. *Phys. Rev. Lett.*, 112(3):030602, 2014.
- [15] Obinna Abah and Eric Lutz. Optimal performance of a quantum otto refrigerator. *EPL*, 113(6):60002, 2016.
- [16] Henry ED Scovil and Erich O Schulz-DuBois. Three-level masers as heat engines. *Phys. Rev. Lett.*, 2(6):262, 1959.
- [17] Robert Alicki. The quantum open system as a model of the heat engine. *J. Phys. A*, 12(5):L103, 1979.
- [18] Ronnie Kosloff. A quantum mechanical open system as a model of a heat engine. *chem. phys.*, 80(4):1625–1631, 1984.
- [19] Yanchao Zhang. Optimization performance of quantum otto heat engines and refrigerators with squeezed thermal reservoirs. *Physica A*, 559:125083, 2020.
- [20] Rui Wang, Jianhui Wang, Jizhou He, and Yongli Ma. Efficiency at maximum power of a heat engine working with a two-level atomic system. *Phys. Rev. E*, 87(4):042119, 2013.

- [21] Sai Vinjanampathy and Janet Anders. Quantum thermodynamics. *Contemp. Phys.*, 57(4):545–579, 2016.
- [22] Ashutosh Kumar, Trilochan Bagarti, Sourabh Lahiri, and Subhashish Banerjee. Thermodynamics of one and two-qubit nonequilibrium heat engines running between squeezed thermal reservoirs. *Physica A*, page 128832, 2023.
- [23] Zijun Yan and Jincan Chen. A class of irreversible carnot refrigeration cycles with a general heat transfer law. *J. Phys. D: Appl. Phys.*, 23(2):136, 1990.
- [24] Varinder Singh, Tanmoy Pandit, and Ramandeep S Johal. Optimal performance of a three-level quantum refrigerator. *Phys. Rev. E*, 101(6):062121, 2020.
- [25] Zbigniew Ficek and Ryszard Tanaś. Entangled states and collective nonclassical effects in two-atom systems. *Phys. Rep*, 372(5):369–443, 2002.
- [26] Subhashish Banerjee, V Ravishankar, and R Srikanth. Dynamics of entanglement in two-qubit open system interacting with a squeezed thermal bath via dissipative interaction. *Ann. Phys.*, 325(4):816–834, 2010.
- [27] Subhashish Banerjee. *Open quantum system: Dynamics of nonclassical evolution*. springer, 2019.
- [28] Heinz-Peter Breuer and Francesco Petruccione. *The theory of open quantum systems*. Oxford University Press, 2002.
- [29] Gonzalo Manzano. Squeezed thermal reservoir as a generalized equilibrium reservoir. *Phys. Rev. E*, 98(4):042123, 2018.
- [30] Santiago Velasco, José MM Roco, Alejandro Medina, and A Calvo Hernández. New performance bounds for a finite-time carnot refrigerator. *Phys. Rev. Lett.*, 78(17):3241, 1997.
- [31] Armen E Allahverdyan, Karen Hovhannisyanyan, and Guenter Mahler. Optimal refrigerator. *Phys. Rev. E*, 81(5):051129, 2010.
- [32] C De Tomás, A Calvo Hernández, and JMM Roco. Optimal low symmetric dissipation carnot engines and refrigerators. *Phys. Rev. E*, 85(1):010104, 2012.